



Impact of multiscale variability on last 6,000 years Indian and West African monsoon rain.

Pascale Braconnot, Julien Crétat, O. Marti, Yves Balkanski, A. Caubel, A. Cozic, Marie-Alice Foujols, S. Sanogo

► To cite this version:

Pascale Braconnot, Julien Crétat, O. Marti, Yves Balkanski, A. Caubel, et al.. Impact of multiscale variability on last 6,000 years Indian and West African monsoon rain.. Geophysical Research Letters, 2019, 46 (23), pp.14021-14029. 10.1029/2019GL084797 . hal-02615396

HAL Id: hal-02615396

<https://hal.science/hal-02615396>

Submitted on 17 Sep 2020

HAL is a multi-disciplinary open access archive for the deposit and dissemination of scientific research documents, whether they are published or not. The documents may come from teaching and research institutions in France or abroad, or from public or private research centers.

L'archive ouverte pluridisciplinaire **HAL**, est destinée au dépôt et à la diffusion de documents scientifiques de niveau recherche, publiés ou non, émanant des établissements d'enseignement et de recherche français ou étrangers, des laboratoires publics ou privés.



Geophysical Research Letters

RESEARCH LETTER

10.1029/2019GL084797

Key Points:

- Indian monsoon rainfall is more sensitive than West African monsoon rainfall to CO₂
- Two major bands of chaotic variability, 2–20 years and 50–500 years, affect Indian and West African monsoon variability of the last 6,000 years
- Opposite Holocene variability trends in Indian and African monsoon are due to interannual and not centennial variability linkages with mean state

Supporting Information:

- Supporting Information S1

Correspondence to:

P. Braconnot,
pascale.braconnot@lsce.ipsl.fr

Citation:

Braconnot, P., Crétat, J., Marti, O., Balkanski, Y., Caubel, A., Cozic, A., et al. (2019). Impact of multiscale variability on last 6,000 Years Indian and West African monsoon rain. *Geophysical Research Letters*, 46, 14,021–14,029. <https://doi.org/10.1029/2019GL084797>

Received 6 AUG 2019

Accepted 19 NOV 2019

Accepted article online 22 NOV 2019

Published online 4 DEC 2019

Impact of Multiscale Variability on Last 6,000 Years Indian and West African Monsoon Rain

P. Braconnot¹, J. Crétat^{1,2}, O. Marti¹, Y. Balkanski¹, A. Caubel¹, A. Cozic¹, M.-A. Foujols³, and S. Sanogo^{1,4}

¹Laboratoire des Sciences du climat et de l'environnement-IPSL, Unité Mixte CEA-CNRS-UVSQ, Université Paris-Saclay, Orme des Merisiers, Gif-sur-Yvette, France, ²Centre de Recherche de Climatologie, UMR6282 Biogéosciences, Dijon, France, ³Institut Pierre Simon Laplace, Sorbonne Université, Paris, France, ⁴Centre National de la Recherche Météorologique, Toulouse, France

Abstract Particularly dry or wet boreal summer monsoon seasons are major hazards affecting societal vulnerability in India and Africa. Several factors affect monsoon rainfall amount and limit the understanding of possible linkages between monsoon variability and mean climate changes. Here we characterize the multiscale variability of Indian and West African monsoon rain from two simulations of the last 6,000 years. Changes in Earth's orbit cause long-term monsoon drying trend in India and Africa, but the Indian monsoon is more sensitive to anthropogenic CO₂. Variability is characterized by two major ranges of chaotic variability, each related to specific ocean-atmosphere modes present throughout the period. Combination of random 50- to 500- and 2- to 20-year variability leads to large events occurring at millennium scale. However, the two regions exhibit opposite trends in rainfall variability due to changes in teleconnection with Pacific sea surface temperature for India and Atlantic sea surface temperature for West Africa at interannual to decadal timescales.

1. Introduction

Monsoon is a key feature of the seasonal cycle in the tropics. It accounts for more than 55% of the annual mean precipitation in India and West Africa (Wang & Ding, 2008). A full understanding of the monsoon interannual variability from the recent well-observed period is however difficult. The records span over too short a time to sample the wide range of variability and are affected by global warming induced by human activity (Hartmann et al., 2013). The paleoclimate records offer a longer perspective. They indicate that the Northern Hemisphere monsoon rain belt penetrated further north into the continent 6,000 years BP (Masson-Delmotte et al., 2013; Mohtadi et al., 2016) and gradually retreated back to its modern condition (Wanner et al., 2008). Depending on the region, this retreat appears as abrupt or rapid (deMenocal et al., 2000; Fleitmann et al., 2003; Z Liu et al., 2007). Records also point to mega droughts and events that had a profound impact on civilization in the Indus Valley (Kathayat et al., 2017; Staubwasser et al., 2003) or in the Sahara-Sahel region during the end of the African Humid period (Kuper & Kröpelin, 2006). Changes in variability have also been reported for the El Niño–Southern Oscillation (ENSO) (Carre et al., 2014; Cobb et al., 2013; Emile-Geay et al., 2016) and the North Atlantic Oscillation (NAO) (Olsen et al., 2012). These climate variability modes have been shown to affect monsoon rain in the modern era and are suspected to have affected past monsoon rain (Z Y Liu et al., 2006; Yan & Liu, 2019; Zhao et al., 2007). However, high-resolution paleorecord syntheses that span over the last 6,000 years are still too limited, and most of them do not have yet the resolution needed to properly disentangle the role of the different timescales and teleconnections affecting monsoon variability at interannual to multicentennial timescales. In addition, previous studies did not consider the relative influence of main modes of ocean-atmosphere variability while considering both Indian and West African monsoons during the Holocene.

Here, we make use of new possibilities provided by long transient climate simulations to characterize the multiscale variability of the Indian and West African. Two simulations of the last 6,000 years enable us to analyze robust climate mean state responses to the orbital and trace gas forcing and possible relationships between mean state and changes in interannual to multicentennial variability. The aims are to isolate different timescales and modes of variability affecting Indian and West African monsoon rainfall and determine whether variability changes with time are chaotic or depend on changes in the mean state. An important

point here is thus to consider simultaneously the two monsoon systems to extract modes of in-phase and out-of-phase covariations at the different timescales throughout the last 6,000 years. These analyses are a prerequisite prior to detailed analyses of variability combining model and paleoclimate reconstructions when different variabilities interfere together to produce the resulting environmental changes.

We introduce the simulations in section 2. Section 3 emphasizes the long-term changes in rainfall mean state and variability, while section 4 discusses two major variability timescales affecting monsoon variability, as well as variability trends and the associated teleconnections. The conclusions are provided in section 5.

2. Materials and Methods

2.1. Model and Experiments

We used two versions of the IPSL model to run the transient simulations of the last 6,000 years (Braconnot et al., 2019; Dufresne et al., 2013). This state-of-the-art general circulation model represents the three-dimensional circulation of the atmosphere and the ocean, the land surface, and the interactions between climate and the carbon cycle. The first simulation, called S-Vlr01, was run with the IPSLCM5A-LR version (Dufresne et al., 2013) used to produce the set of past, present and future CMIP5 simulations (Taylor et al., 2012) considered as reference for the IPCC AR5 report (IPCC, 2013). The atmospheric model resolution is 3.75° in longitude, 1.875° in latitude, and 39 vertical levels. The ocean model resolution is 2° , with spatial refinement at the equator and in the Arctic, and 31 vertical levels. The second simulation, V-Sr02, was run with a modified version and the medium resolution of IPSLCM5A (IPSLCM5A-MR) with an atmospheric horizontal resolution of 2.5° in longitude and 1.125° in latitude (Braconnot et al., 2019). A new 11-layer soil hydrology, a prognostic snow model, and a dynamical vegetation module have been introduced in the land surface component, allowing vegetation types to vary in each grid box (Braconnot et al., 2019).

The initial state of each experiment comes from a 1,000-year-long simulation performed with the corresponding model version and the Paleoclimate Modeling Intercomparison Project 6,000 years BP boundary conditions (Kageyama et al., 2018). Then, Earth's orbital parameters and atmospheric composition derived from ice-core reconstructions (Otto-Bliesner et al., 2017) were updated each year from 6,000 ka BP to 0 ka BP (1950 which is the reference for Earth's orbital parameters; Berger, 1978).

2.2. Analyses of Monsoon Variability

Area-averaged precipitation and sea surface temperature (SST) indices have been selected to reduce the dimensionality of the large space-time fields. Their combined analysis is designed to detect the major factors constraining changes in variability over the last 6,000 years. In addition to the Indian (ISMR) and West African (WAMR) monsoon rainfall indices (Figure 1), we considered SST indices commonly used to investigate interannual-to-multidecadal teleconnections with the two monsoon systems (Hartmann et al., 2013). We kept standard modern definitions of these indices since the corresponding regions have also large interannual variance in the simulations and are large enough to account for small variability shifts over the last 6,000 years. Possible shifts in the simulations due to model SST biases or due to small changes in variability domains with time do not alter the results. The different indices are defined as follow (supporting information Figure S1): ISMR: $5\text{--}25^{\circ}\text{N}$; $70\text{--}88^{\circ}\text{E}$ (land points); WAMR: $7\text{--}18^{\circ}\text{N}$; 15°W to 20°E (land points); AMO (Atlantic multidecadal oscillation): difference between North Atlantic SST (equator to 60°N ; 80°W to 0) and global SST in the 60°S to 60°N band; MED (Mediterranean): $30\text{--}50^{\circ}\text{N}$; 8°W to 45°E ; NTA (North tropical Atlantic): 5°S to 25°N ; $55\text{--}15^{\circ}\text{W}$; STA (South tropical Atlantic): 20°S to equator; 30°W to 10°E ; AD (Atlantic dipole): NTA minus STA; ATL3 (tropical Atlantic): 3°S to 3°N ; 20°W to 0; WIOD (west Indian Ocean dipole): 10°S to 10°N ; $50\text{--}70^{\circ}\text{E}$; EIOD (east Indian Ocean dipole): 10°S to equator; $90\text{--}110^{\circ}\text{E}$; IOD: (Indian Ocean dipole): WIOD minus EIOD; NINO34 (Niño 3.4 region): 5°S to 5°N ; $170\text{--}120^{\circ}\text{W}$.

We now characterize the modes of variability between the two monsoon indices and SST through empirical orthogonal function (EOF) applied to June-to-September seasonal rainfall and SST indices filtered in different variability bands (see supporting Figures S2 to S4 and Tables S1–S3 for complements). All time series are standardized prior to the EOF analyses to account for the different units. The EOF space offers a reduced dimensional space in which key factors contributing to ISMR and WAMR variability can be isolated. These analyses are thus used as a guideline to pinpoint the main modes of monsoon variability and the

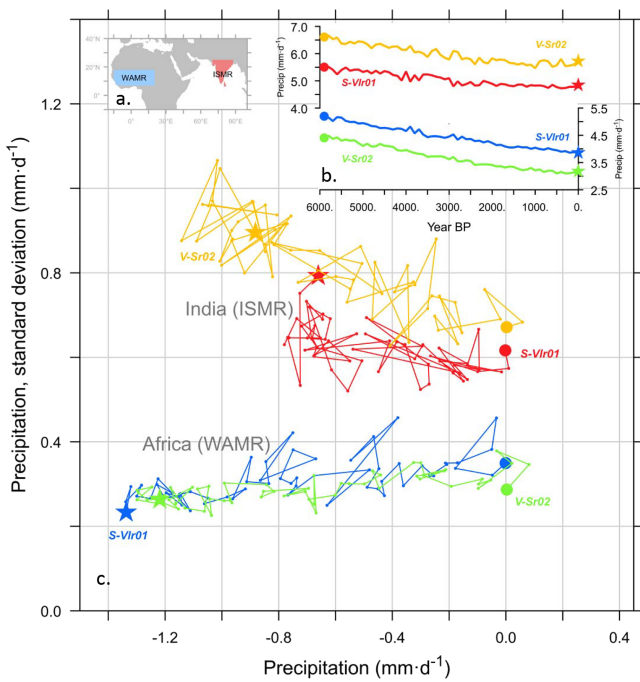


Figure 1. Evolution of the simulated Indian and West African precipitation over the last 6,000 years, showing similar long-term trends but opposite variability trends between the two monsoon regions. (a) Location of the regions used to compute the Indian (ISMР: red) and West African (WAMR: blue) precipitation indices. (b) ISMR and WAMR evolution (mm day^{-1}) over the last 6,000 years, smoothed with a 100-year running mean. (c) Relationship between the long-term changes (100-year mean departure from mid-Holocene conditions; x axis) and the variability (estimated by the standard deviation) in 100-year successive windows (y axis) for each region and each simulation. For each region, the curves show the results for the two simulations, in red and blue for S-Vlr01 and in orange and green for V-Sr02.

major factors controlling the diversity of events affecting ISMR and WAMR. We do not intend to go into a detailed discussion of the variability and of the small relative variations between all the indices or between the two simulations.

Regarding SST, we considered both dipole indices and the two indices used to define these dipoles in the Atlantic and Indian Ocean because they provide additional information. The total number of degrees of freedom is thus 10 (12 corresponding to the total number of indices—1 for the mean — $2^*0.5$ for the correlation between dipole indices and boxes). We expect thus at most 10 eigenvalues different from 0. Using equation (1) below allows to reconstruct the time series of precipitation and SST indices (listed above) from the EOF:

$$\text{reconstructed index}(t) = \sum_{i=1}^{10} a_i(t) * \text{EOF}_{\text{index}}, \quad (1)$$

with t corresponding to each of the 6,000 July-to-September seasons, i the EOF mode from 1 to 10, a the EOF eigenvector, and $\text{EOF}_{\text{index}}$, the EOF load for the corresponding index. The number of times an EOF mode is dominant in a 500-year window can also be estimated for each rainfall and SST index. This is done by extracting at each time step t the EOF with the largest absolute value of $a_i(t)$. Then, for each EOF mode, we count the number of times it dominates in 500-year adjacent windows.

Applying the method to the last 100 years of the simulations and observational products give confidence that, despite some common biases, both model versions have some skill in reproducing ISMR and WAMR and large scale monsoon teleconnection at 2- to 20-year variability timescale (see supporting information Figure S5).

3. Long-Term Indian and African Monsoon Trends

3.1. Mean Trend

Figure 1 shows that, despite different mean ISMR and WAMR amounts between the two simulations, they produce the drying trend induced by the slow variations in Earth's orbit (Joussaume et al., 1999; Z Liu et al., 2004; Zhao & Harrison, 2011; Zhao et al., 2005). It represents about 17–18% of the mean ISMR averaged over the last 6,000 years and 29–36% of the mean WAMR depending on the simulation. The last 100 years of the simulations (i.e., 1850–1950) are characterized by a global warming induced by the rapid increase of the atmospheric greenhouse gases since the beginning of the industrial revolution. The increased greenhouse gases act to slightly offset the long-term cooling in the NH and to amplify the long-term warming in the SH (Braconnot et al., 2019). Slight differences in shape are found between the two regions. Few changes occur in the last 3,000 years for ISMR, whereas the drying trend is still effective for WAMR (Figure 1). We first applied an EOF analysis considering the 500-year low-pass-filtered monsoon and SST indices presented in section 2 to better characterize the monsoon response to the orbital and trace gases forcing. The first two EOF modes are statistically significant and represent respectively 74–69% and 23–29% of the total variance (see supporting information Table S1). Their associated principal components (time series of Figure 2a) resemble respectively the long-term evolution of insolation and trace gas forcing (Braconnot et al., 2019). They are very similar between the two simulations and characterize well the simulated long-term precipitation trends (Figure 1).

The spatial pattern of the first EOF mode reflects the long-term drying trend of ISMR and WAMR that is associated with the cooling of the NH and the warming of the SH, as well as a reduction of the Atlantic and Indian dipoles (Figure 2b). Note that the reduction in strength of the IOD with time is mainly due to eastern Indian Ocean warming (Figure 2b). The SST pattern associated with the second EOF mode (Figure 2c) shares similarities with the impact of the ongoing increase in trace gases on SST (IPCC, 2013).

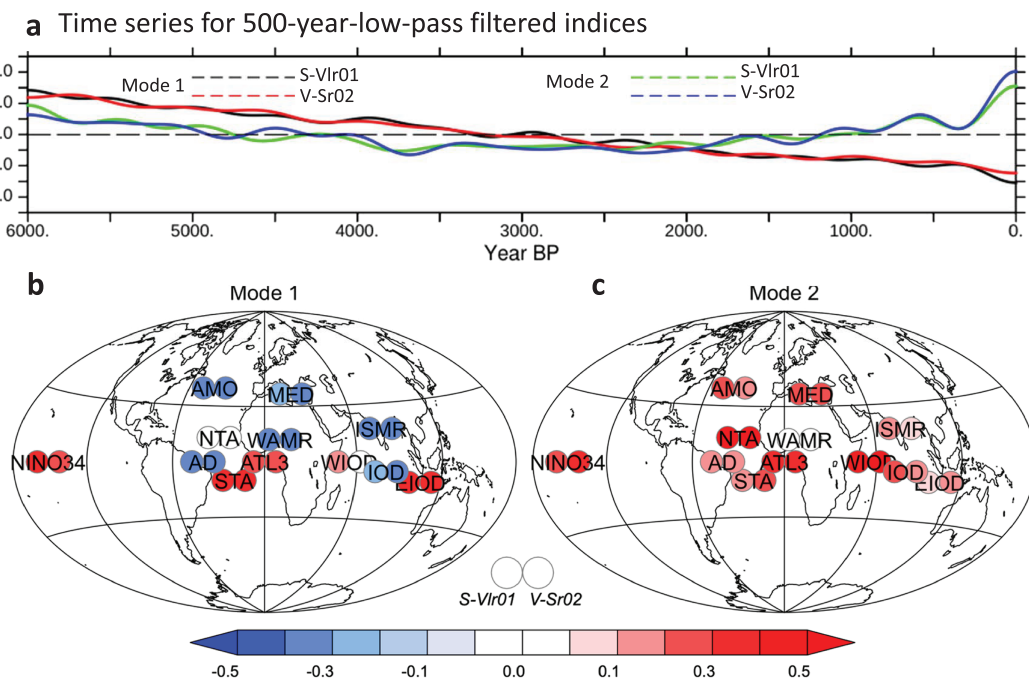


Figure 2. First two modes of long-term changes induced by orbital and trace gas forcing estimated by the Empirical Orthogonal Function analysis of the cross-correlation matrix between 500-year low-pass-filtered monsoon and SST indices. (a) Time series (principal components) of the first two modes for the two simulations. (b) Eigenvectors associated to the first EOF mode (Mode 1) for the two simulations showing the variation of the different indices (relative unit). This mode reflects the long-term response to insolation. (c) Same as (b) but for the second EOF mode that reflects the long-term response to trace gases. The eigenvectors in (b) and (c) represent a unit vector. For each index, the results for S-Vlr01 are plotted on the left circle and those of V-Sr02 on the right circle. The name of the boxes (see section 2.2) is plotted on top of the circles.

It is characterized by increased SST almost everywhere with a relative maximum in the tropical band and in the Indian Ocean (Roxy et al., 2014). Around 3,000–2,500 years ago, insolation and trace gases forcings become of similar order of magnitude. The effect of CO₂ has a larger impact on ISMR than on WAMR and partially counteracts the effect of the insolation forcing on ISMR from 2,500 to 100 years BP before becoming the dominant signal. These two simulations suggest thus that in the absence of land use and aerosols ISMR would have increased from 1850 to 1950 and should increase in the future when the CO₂ effect becomes dominant.

3.2. Variability Trend

Both simulations exhibit a wide range of variability not present in the imposed insolation or trace gases forcing (Figure 1). It appears from internal interactions between all the components of the climate system. Consistent with results of long preindustrial simulations (Wittenberg, 2009), periods with high or low variability are randomly distributed in time. Despite the chaotic nature of variability and the common drying trend, variability in 100-year windows increases with time in India and decreases in West Africa (Figure 1). To further quantify these variability changes, we analyzed the probability to get a wet or a dry ISMR or WAMR season in 100-year windows. To do this analysis, we subtracted the 500-year low-pass-filtered time series from the raw time series and computed, for each 100-year window, the fraction of boreal summer seasons (July-to-September) where seasonal rainfall amounts exceed one (minus one) standard deviation determined over the whole 6,000-year period. This fraction increases with time over India by about 10% and decreases by the same amount over West Africa (see also supporting information Figure S6). This reveals that changes in the variability with time are related to changes in the mean state but that the variability trend does not simply follow the evolution of the mean precipitation.

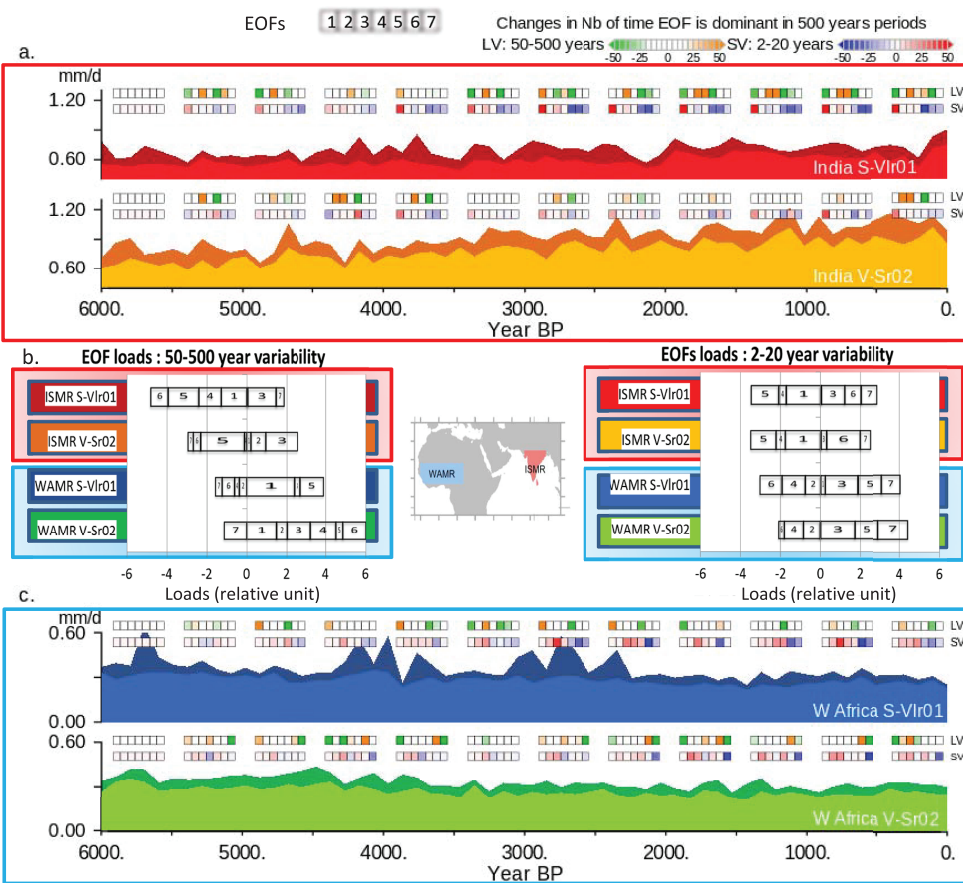


Figure 3. Characterization of the interannual-to-centennial variability of Indian and West African monsoon indices over the last 6,000 years. (a) Standard deviation of the Indian precipitation index filtered in the 2- to 20-year and 50- to 500-year ranges in consecutive 100-year windows. The 50- to 500-year variability is plotted on top of the 2- to 20-year variability to foster comparisons of their relative magnitude. For each 500-year nonoverlapping windows, the seven colored squares show the changes in the respective influence of the first seven EOF modes for the two variability timescales refer to as SV (short term) for the 2- to 20-year variability and LV (long term) for the 50- to 500-year variability (see section 2.2 for analysis details). (b) Loads (relative units) of the first seven EOF modes associated with the Indian (red) and West African (blue) monsoon regions for the 50- to 500-year variability range on the left and the 2- to 20-year variability range on the right. The EOF numbers are plotted on the bars that have a size proportional to the load (relative unit) of each EOF mode for the respective monsoon indices. (c) Same as (a) but for the West African precipitation index. Each region, simulation, and timescales are represented with the same color in all panels. Results of the S-Vlr01 simulation are thus reproduced with red for ISMR and a blue for WAMR as in Figure 1, and the V-Sr02 with orange for ISMR and green for WAMR. The dark versus light colors correspond respectively to the 50- to 500-year and 2- to 20-year variability.

4. Characterization of Multiscale Variability

4.1. Two Major Ranges of Variability

Spectral and wavelet analyses of the monsoon indices further highlight that two major ranges of variability, 2–20 years (SV) and 50–500 years (LV), emerge from red noise (Figure 3 and supporting information Figure S7). In both simulations the 2- to 20-year variability has the largest imprint on monsoon rain (Figures 3a and 3c) and is at the origin of the variability trend depicted in Figure 1. It also implies that the relative weight on the two types of variability varies with time, the 50- to 500-year variability having a larger impact in India during mid-Holocene (Figure 3a) and in West Africa during the last part of the simulations (Figure 3c). Over any period of time, the 50- to 500-year variability induces long peak-to-peak precipitation modulation of the order of $1.2 \text{ mm}\cdot\text{day}^{-1}$ (i.e., as large as the total drying over the last 6,000 years on top of which the 2- to 20-year variability randomly adds peak-to-peak variations reaching up to $4\text{--}5 \text{ mm}\cdot\text{day}^{-1}$ (supporting information Figure S7) when 100-year standard deviation in Figure 3 exhibits

higher values. Random phasing between these two variability ranges alone can thus be involved to understand the major events that had profound impact in the tropics, such as the 4.2 ka BP event (Giesche et al., 2019; Staubwasser et al., 2003).

We further explore the monsoon teleconnection for these two variability timescales by analyzing the cross variations between the two monsoons and the SST indices successively in the two variability bands. Four and five significant EOF modes need to be accounted for to represent about 80% of the total cross correlation between monsoon and SST indices in the 50- to 500-year and 2- to 20-year bands, respectively (supporting information Tables S2 and S3). The leading modes are not necessarily those with major impact on monsoon rainfall (Figure 3b), meaning that local or regional factors also play a significant role on both ISMR and WAMR and that some of the major ocean modes do not affect these monsoon regions. Each of these modes represents particular combinations of SST variability and compound events affecting monsoon rain. We identified in each 500-year period the number of times each EOF mode is dominant in the reconstruction of the ISMR and WAMR variability (colored squares in Figures 3a and 3c). The chance to have one or the other of these modes present in a particular 500-year period randomly varies with time (Figures 3a and 3c). In addition, the patterns associated with 50- to 500-year variability modes differ between the two simulations (supporting information Figure S2). For instance, the first 50–500 EOF mode has a substantial impact on WAMR in both simulations, which is reflected in Figure 3b by the fact that the bars with Number 1 written on them have a significant length for both simulations, even though this EOF1 load is larger for S-Vlr01. This mode is characterized by a robust Atlantic seesaw pattern that favors the north/south migration of the Intertropical Convergence Zone over the ocean and of the monsoon rain belt in West Africa. The EOF1 loadings on the SST indices in the other basins are different between the simulations, which induces a significantly contribution of EOF1 to ISMR variability in S-Vrl01 but not in V-Sr02 (Figure 3b; see also supporting information Figure S2). Similar finding prevails for the other modes. This highlights that the 50- to 500-year variability is driven by basin modes that have different relative phases between the two simulations, as seen by the random distribution of the dominant EOFs in 500-year windows (Figure 3b). Since there are no major events in sea ice or thermohaline circulation, we conclude that these 50- to 500-year modes correspond to basin mode induced by stochastic atmospheric forcing (Hasselmann, 1976). Nonetheless, even if the exact rank of EOF modes affecting respectively WAMR and ISMR 50- to 500-year variability are different between the two simulations, those inducing the largest changes in variability from one 500-year period to the other involve Atlantic seesaw variability for WAMR and a teleconnection between South Atlantic, Indian and Pacific Oceans for ISMR in both simulations. The relative phase of these two major teleconnections is thus a key factor to reproduce relative long-term monsoon variations between ISMR and WAMR. The difficulty for future inference from paleoclimate archives is that they share some similarities with the 2- to 20-year variability that has larger amplitude.

4.2. Trends in the 2- to 20-Year Variability

The modes associated with the 2- to 20-year variability are very similar between the two simulations, even for high number EOFs (Figure 3b; see also supporting information Figure S3). The 6,000 years of simulation offer a large sampling of the 2- to 20-year variability, with 2 to ~10 times more events than in the 50- to 500-year band. There are thus more possibilities to find similar configurations connecting common variability of the different indices. The reduced space provided by the EOFs is also a powerful tool to identify principal directions contributing to the trends seen in Figures 1 and 3. The first EOF alone reproduces the positive variability trend for ISMR (see corresponding EOF color square for SV lines in Figure 3 and supporting information Figure S4). It represents 37% of ISMR variability (Supporting information Table S2). EOFs 6 and 7 in S-Vlr01 and 7 in V-Sr02 have a negative trend and represent 16% to 26% of WAMR variability (Figure 3b and supporting information Table S2 and Figure S4). For each simulation we regressed the SST and the surface wind at each grid point with the corresponding EOF time series. We then combined the results of the two simulations to infer the robust global patterns affecting ISMR and WAMR 2- to 20-year variability trends by averaging the local regressed anomalies from the two simulations if and only if the regressed anomalies have the same sign and the correlation between corresponding anomalies and EOF time series is significant at the 95% confidence level (Pearson test) in the two simulations (Figure 4). Otherwise, the local ensemble-mean anomaly is considered as nonsignificant and is discarded.

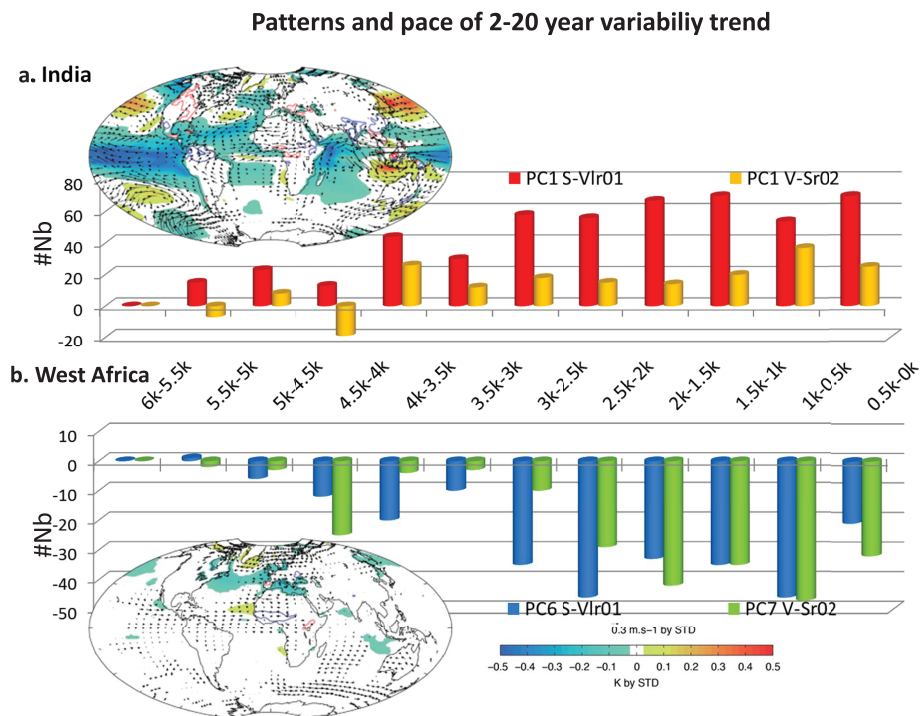


Figure 4. Modes of interannual-to-decadal variability contributing to the last 6,000-year variability increase of the Indian monsoon and decrease of the African monsoon. (a) Ensemble-mean regression patterns onto the first 2- to 20-year EOF mode. Shading stands for SST anomalies (K), arrows for 850-hPa wind anomalies ($m \cdot s^{-1}$) and contours for rainfall anomalies over land (red/blue contours for dry/wet anomalies, with light and dark colors for $|0.1|$ and $|0.5| mm.d^{-1}$ anomalies, respectively). The bars represent the evolution from the mid-Holocene (difference with 6–5.5 ka BP) of the number of times where this pattern is dominant in consecutive 500-year windows for the two simulations. (b) Same as (a) but for EOF Modes 6 and 7 that are related to decreased West African monsoon variability in respectively, S-Vlr01 and V-Sr02. The same colors as in Figures 1 and 3 have been chosen to represent the results of the two simulations for ISMR and WAMR. Note also that the bars reproduce the same information as the one plotted on the corresponding EOF Square on the SV lines in Figure 3 (i.e., the first square for ISMR and Square Number 6 or 7 depending on the simulation for WAMR).

The SST pattern linked to the increase in ISMR 2- to 20-year variability resembles the teleconnection pattern found under modern conditions between ENSO and the Indian monsoon (Figure 4a). It is characterized by cold SST anomalies in the East Pacific and a reduced Indian Ocean dipole (east/west temperature gradient). The anomalous circulation in the Arabian Sea and the Bay of Bengal associated to ENSO variability becomes more frequent and dominant with time, and therefore has a larger impact on ISMR (Figures 3a and 4a). It arises from the combination of the relaxation of interhemispheric and land-sea contrasts induced by the long-term variations of insolation and of the associated increased impact of ENSO on global energetics and teleconnections (Saint-Lu et al., 2016). Note that other 2- to 20-year EOF modes also involve ENSO type patterns in the Pacific, but with different combinations of SST anomalies in the Atlantic and Indian Oceans and no specific trend over the last 6,000 years (supporting information Figures S3 and S4).

The EOF modes contributing to the negative trend in WAMR 2- to 20-year variability are EOF6/EOF7 for S-Vlr01 and EOF7 for V-Sr02 (Figure 3c). These modes have similar patterns over West Africa and the Atlantic sector but differ elsewhere (supporting information Figure S5). This suggests that the decrease in West African monsoon variability arises from regional factors. The regional pattern shared by the two simulations resembles the NAO pattern (Hurrell et al., 2003), except that SST anomalies have a signal larger than observed for modern NAO conditions in the Mediterranean Basin (Figure 4). Wet WAMR anomalies are associated to a SST tripole in the North Atlantic, with warmer conditions west off West Africa and south of Iceland and colder conditions between 40°N and 45°N . Colder than normal SST in the Mediterranean

Sea induces an anomalous cyclonic circulation and the temperature decrease in the tropical Atlantic reinforces the local land-sea temperature contrast and the moisture inflow onto West Africa (Figure 4b). In West Africa, the strength of the subtropical Atlantic dipole reduces in response to the insolation during boreal summer (Figure 2). It induces a southward shift of the rain belt. It also damps the effect of variability by counteracting the effect of the anomalous cyclonic circulation around a colder Mediterranean Sea and enhanced cyclonic inflow from the equator on WAMR (Figure 4).

Figure 4 further highlights that the largest trends in rainfall variability occur between 4.5 and 2.5 ka BP with different relative timing between ISMR and WAMR. The large internal noise makes it difficult to go further, but we can infer that current 2- to 20-year variability conditions are certainly in place since about 2,500 to 3,000 years. We also tested if the 2- to 20-year variability is modulated by the 50- to 500-year variability but found no clear statistical relationship. It is possible that major 50- to 500-year events remain too rare or are not long enough to robustly infer their interplay with the chaotic interannual variability.

5. Conclusions

Our results highlight that interannual-to-decadal variability for the last 6,000 years has opposite trends over India and West Africa and that its interactions with 50- to 500-year variability trigger extreme dry and wet events at the centennial-to-millennium timescale. Because of the wide range of combinations of cross variations between monsoon rain and ocean variability, a long-term perspective is the only way to properly assess this diversity and the origin of variability trend. These results are consistent with our knowledge of the 2- to 20-year ENSO variability and emerge despite the chaotic nature of this 2- to 20-year variability in two simulations with different model versions and complexity. We are confident to have identified a robust signal that would benefit from future model-data comparisons. Our results bring into light new information about monsoon variability. The chaotic nature of 50- to 500-year Holocene variability has already been evidenced over Europe (Marsicek et al., 2018). It is such that there is little chance to capture together the climate trajectory recorded in paleoclimate archive, except in regions where water resources are close to a threshold allowing variability to trigger rapid changes of its environment. Disentangling the role of the two variability ranges is thus important to better understand monsoon changes and being able to properly combine information for different types of paleoclimate archives. Our results reveal the different behavior of 50- to 500-year and 2- to 20-year monsoon rainfall variability as well as the fact that we only detect linkages between 2- to 20-year monsoon rainfall variability and changes in the long-term climate mean state. They open perspectives to anticipate changes in extreme dry or wet monsoon seasons and to derive relevant adaptation criteria in each specific monsoon context.

Acknowledgments

We acknowledge PRACE for awarding us access to Curie at GENCI@CEA, France (THROL project) to start the simulations. The simulations were also performed using HPC resources from GENCI-TGCC thanks to a high-end computing access grant and to our annual allocation time (gen2212). This work is supported by the JPI-Belmont PACMEDY project (ANR-15-JCLI-0003-01). It benefits from the development of the common modeling IPSL infrastructure coordinated by the IPSL climate modeling center (<https://cmc.ipsl.fr/>). The Ferret program was used for analysis and graphics in this paper. Ferret is a product of NOAA's Pacific Marine Environmental Laboratory (Information is available at <http://ferret.pmel.noaa.gov/Ferret>). Authors declare no competing interests. The outputs of the simulations used in this manuscript are freely available (<https://doi.org/10.14768/20191028001.1>).

References

- Berger, A. (1978). Long-term variations of caloric solar radiation resulting from the Earth's orbital elements. *Quaternary Research*, 9, 139–167.
- Braconnot, P., Zhu, D., Marti, O., & Servonnat, J. (2019). Strengths and challenges for transient Mid- to Late Holocene simulations with dynamical vegetation. *Climate of the Past*, 15(3), 997–1024. <https://doi.org/10.5194/cp-15-997-2019>
- Carre, M., Sachs, J. P., Purca, S., Schauer, A. J., Braconnot, P., Falcon, R. A., et al. (2014). Holocene history of ENSO variance and asymmetry in the eastern tropical Pacific. *Science*, 345(6200), 1045–1048. <https://doi.org/10.1126/science.1252220>
- Cobb, K. M., Westphal, N., Sayani, H. R., Watson, J. T., Di Lorenzo, E., Cheng, H., et al. (2013). Highly variable El Niño–Southern Oscillation throughout the Holocene. *Science*, 339(6115), 67–70. <https://doi.org/10.1126/science.1228246>
- deMenocal, P., Ortiz, J., Guilderson, T., Adkins, J., Sarnthein, M., Baker, L., & Yarusinsky, M. (2000). Abrupt onset and termination of the African Humid Period: Rapid climate responses to gradual insolation forcing. *Quaternary Science Reviews*, 19(1–5), 347–361. [https://doi.org/10.1016/s0277-3791\(99\)00081-5](https://doi.org/10.1016/s0277-3791(99)00081-5)
- Dufresne, J. L., Foujols, M. A., Denvil, S., Caubel, A., Marti, O., Aumont, O., et al. (2013). Climate change projections using the IPSL-CM5 Earth System Model: From CMIP3 to CMIP5. *Climate Dynamics*, 40(9–10), 2123–2165. <https://doi.org/10.1007/s00382-012-1636-1>
- Emile-Geay, J., Cobb, K. M., Carré, M., Braconnot, P., Leloup, J., Zhou, Y., et al. (2016). Links between tropical Pacific seasonal, interannual and orbital variability during the Holocene. *Nature Geoscience*, 9(2), 168–173. <https://doi.org/10.1038/ngeo2608>
- Fleitmann, D., Burns, S. J., Mudelsee, M., Neff, U., Kramers, J., Mangini, A., & Matter, A. (2003). Holocene forcing of the Indian monsoon recorded in a stalagmite from southern Oman. *Science*, 300(5626), 1737–1739.
- Giesche, A., Staubwasser, M., Petrie, C. A., & Hodell, D. A. (2019). Indian winter and summer monsoon strength over the 4.2 ka BP event in foraminifer isotope records from the Indus River delta in the Arabian Sea. *Climate of the Past*, 15(1), 73–90. <https://doi.org/10.5194/cp-15-73-2019>
- Hartmann, D. L., A. M. K. Tank, M. Rusticucci, L. V. Alexander, S. Brönnimann, Y. A. R. Charabi, et al. (2013). Observations: Atmosphere and surface. In T. F. Stocker, D. Qin, G.-K. Plattner, M. Tignor, S. K. Allen, J., Boschung et al. (Eds.). *Climate change 2013 the physical science basis: Working Group I contribution to the fifth assessment report of the intergovernmental panel on climate change* (pp. 159–254). Cambridge, UK and New York, USA: Cambridge University Press.
- Hasselmann, K. (1976). Stochastic climate models Part I. Theory. *Tellus*, 28(6), 473–485. <https://doi.org/10.3402/tellusa.v28i6.11316>

- Hurrell, J. W., Kushnir, Y., & Ottersen, G. (2003). An overview of the North Atlantic Oscillation. In Y. K. J. W. Hurrell, G. Ottersen, M. Visbeck, & M. H. Visbeck (Eds.), *the North Atlantic Oscillation: Climatic significance and environmental impact, Environmental Impact* (pp. 1–35). Washington: American Geophysical Union. <https://doi.org/10.1029/134GM01>
- IPCC (2013). *Climate Change 2013—The physical science basis. Working Group I Contribution to the Fifth Assessment Report of the IPCC* (p. 1535). Cambridge, United Kingdom and New York, NY, USA: Cambridge University Press.
- Joussaume, S., Taylor, K. E., Braconnot, P., Mitchell, J. F. B., Kutzbach, J. E., Harrison, S. P., et al. (1999). Monsoon changes for 6000 years ago: Results of 18 simulations from the Paleoclimate Modeling Intercomparison Project (PMIP). *Geophysical Research Letters*, 26(7), 859–862. <https://doi.org/10.1029/1999gl900126>
- Kageyama, M., Braconnot, P., Harrison, S. P., Haywood, A. M., Jungclaus, J. H., Otto-Bliesner, B. L., et al. (2018). The PMIP4 contribution to CMIP6-Part 1: Overview and over-arching analysis plan. *Geoscientific Model Development*, 11(3), 1033–1057. <https://doi.org/10.5194/gmd-11-1033-2018>
- Kathayat, G., Cheng, H., Sinha, A., Yi, L., Li, X., Zhang, H., et al. (2017). The Indian monsoon variability and civilization changes in the Indian subcontinent. *Science Advances*, 3(12), e1701296. <https://doi.org/10.1126/sciadv.1701296>
- Kuper, R., & Kröpelin, S. (2006). Climate-controlled Holocene occupation in the Sahara: Motor of Africa's evolution. *Science*, 313(5788), 803–807. <https://doi.org/10.1126/science.1130989>
- Liu, Z., Harrison, S. P., Kutzbach, J., & Otto-Bliesner, B. (2004). Global monsoons in the mid-Holocene and oceanic feedback. *Climate Dynamics*, 22(2–3), 157–182.
- Liu, Z., Wang, Y., Gallimore, R., Gasse, F., Johnson, T., deMenocal, P., et al. (2007). Simulating the transient evolution and abrupt change of Northern Africa atmosphere-ocean-terrestrial ecosystem in the Holocene. *Quaternary Science Reviews*, 26(13–14), 1818–1837. <https://doi.org/10.1016/j.quascirev.2007.03.002>
- Liu, Z. Y., Wang, Y., Gallimore, R., Notaro, M., & Prentice, I. C. (2006). On the cause of abrupt vegetation collapse in North Africa during the Holocene: Climate variability vs. vegetation feedback. *Geophysical Research Letters*, 33, L22709. <https://doi.org/10.1029/2006GL028062>
- Marsicek, J., Shuman, B. N., Bartlein, P. J., Shafer, S. L., & Brewer, S. (2018). Reconciling divergent trends and millennial variations in Holocene temperatures. *Nature*, 554(7690), 92–96. <https://doi.org/10.1038/nature25464>, <https://www.nature.com/articles/nature25464#supplementary-information>
- Masson-Delmotte, V., Schulz, M., Abe-Ouchi, A., Beer, J., Ganopolski, A., González Rouco, J., et al. (2013). Information from paleoclimate archives: Chapter 5. In T. F. Stocker, D. Qin, G.-K. Plattner, M. Tignor, S. K. Allen, J. Doschung, et al. (Eds.), *Climate Change 2013: The Physical Science Basis. Contribution of Working Group I to the Fifth Assessment Report of the Intergovernmental Panel on Climate Change* (pp. 383–464). Cambridge: Cambridge University Press.
- Mohtadi, M., Prange, M., & Steinke, S. (2016). Palaeoclimatic insights into forcing and response of monsoon rainfall. *Nature*, 533(7602), 191–199. <https://doi.org/10.1038/nature17450>
- Olsen, J., Anderson, N. J., & Knudsen, M. F. (2012). Variability of the North Atlantic Oscillation over the past 5,200 years. *Nature Geoscience*, 5(11), 808–812.
- Otto-Bliesner, B., Braconnot, P., Harrison, S. P., Lunt, D. J., Abe-Ouchi, A., Albani, S., et al. (2017). The PMIP4 contribution to CMIP6—Part 2: Two interglacials, scientific objective and experimental design for Holocene and Last Interglacial simulations. *Geoscientific Model Development*, 10(11), 3979–4003. <https://doi.org/10.5194/gmd-10-3979-2017>
- Roxy, M. K., Ritika, K., Terray, P., & Masson, S. (2014). The curious case of Indian Ocean warming. *Journal of Climate*, 27(22), 8501–8509. <https://doi.org/10.1175/jcli-d-14-00471.1>
- Saint-Lu, M., Braconnot, P., Leloup, J., & Martí, O. (2016). The role of El Niño in the global energy redistribution: A case study in the mid-Holocene. *Climate Dynamics*, 1–18.
- Staubwasser, M., Sirocko, F., Grootes, P. M., & Segl, M. (2005). Climate change at the 4.2 ka BP termination of the Indus valley civilization and Holocene south Asian monsoon variability. *Geophysical Research Letters*, 30(8), 1425. <https://doi.org/10.1029/2002GL016822>
- Taylor, K. E., Stouffer, R. J., & Meehl, G. A. (2012). An overview of CMIP5 and the experiment design. *Bulletin of the American Meteorological Society*, 93(4), 485–498. <https://doi.org/10.1175/bams-d-11-00094.1>
- Wang, B., & Ding, Q. H. (2008). Global monsoon: Dominant mode of annual variation in the tropics. *Dynamics of Atmospheres and Oceans*, 44(3–4), 165–183. <https://doi.org/10.1016/j.dynatmoce.2007.05.002>
- Wanner, H., Beer, J., Bütkofer, J., Crowley, T. J., Cubasch, U., Flückiger, J., et al. (2008). Mid- to Late Holocene climate change: An overview. *Quaternary Science Reviews*, 27(19–20), 1791–1828. <https://doi.org/10.1016/j.quascirev.2008.06.013>
- Wittenberg, A. T. (2009). Are historical records sufficient to constrain ENSO simulations? *Geophysical Research Letters*, 36, L12702. <https://doi.org/10.1029/2009GL038710>
- Yan, M., & Liu, J. (2019). Physical processes of cooling and mega-drought during the 4.2 ka BP event: Results from TraCE-21 ka simulations. *Climate of the Past*, 15(1), 265–277. <https://doi.org/10.5194/cp-15-265-2019>
- Zhao, Y., Braconnot, P., Harrison, S. P., Yiou, P., & Martí, O. (2007). Simulated changes in the relationship between tropical ocean temperatures and the western African monsoon during the mid-Holocene. *Climate Dynamics*, 28(5), 533–551. <https://doi.org/10.1007/s00382-006-0196-7>
- Zhao, Y., Braconnot, P., Martí, O., Harrison, S. P., Hewitt, C., Kitoh, A., et al. (2005). A multi-model analysis of the role of the ocean on the African and Indian monsoon during the mid-Holocene. *Climate Dynamics*, 25(7–8), 777–800. <https://doi.org/10.1007/s00382-005-0075-7>
- Zhao, Y., & Harrison, S. P. (2011). Mid-Holocene monsoons: A multi-model analysis of the inter-hemispheric differences in the responses to orbital forcing and ocean feedbacks. *Climate Dynamics*, 39(6), 1457–1487. <https://doi.org/10.1007/s00382-011-1193-z>